SAE INTERNATIONAL

An Evaluation of Two Methodologies for Lens Distortion Removal when EXIF Data is Unavailable

2017-01-1422

Published 03/28/2017

Toby Terpstra, Seth Miller, and Alireza Hashemian
Kineticorp LLC

CITATION: Terpstra, T., Miller, S., and Hashemian, A., "An Evaluation of Two Methodologies for Lens Distortion Removal when EXIF Data is Unavailable," SAE Technical Paper 2017-01-1422, 2017, doi:10.4271/2017-01-1422.

Abstract

Photogrammetry and the accuracy of a photogrammetric solution is reliant on the quality of photographs and the accuracy of pixel location within the photographs. A photograph with lens distortion can create inaccuracies within a photogrammetric solution. Due to the curved nature of a camera's lens(s), the light coming through the lens and onto the image sensor can have varying degrees of distortion. There are commercially available software titles that rely on a library of known cameras, lenses, and configurations for removing lens distortion. However, to use these software titles the camera manufacturer, model, lens and focal length must be known. This paper presents two methodologies for removing lens distortion when camera and lens specific information is not available. The first methodology uses linear objects within the photograph to determine the amount of lens distortion present. This method will be referred to as the straight-line method. The second methodology utilizes photogrammetry principles and 3D point cloud data to solve for and remove lens distortion. This method will be referred to as the point cloud method. Using cameras with known distortion parameters, both methodologies are presented and individually evaluated against publically available, library-based, distortion removal solutions. Based on the results of lens distortion removal from cameras with known lens distortion, the straight-line method was found to improve pixel location within a photograph by an average of 82 percent and by as much as 99 percent. The point cloud method was found to improve pixel location by an average of 40 percent and by as much as 66 percent.

Introduction

Photogrammetry is defined by the American Society of Photogrammetry and Remote Sensing (ASPRS) as the art, science, and technology of obtaining reliable information about physical objects and the environment through process of recording, measuring and interpreting photographic images and patterns of recorded radiant electromagnetic energy and other phenomena [1]. The accident reconstruction community has seen the benefit of using photogrammetry in a number of areas for many years. Photogrammetry has proven particularly useful for accident scene diagramming [2, 3, 4, 5, 6, 7, 8, 9, 10, 11, 12, 13, 14, 15, 16, 17, 18, 19, 20], measuring vehicle crush [21, 22, 23, 24, 25, 26, 27], vehicle modeling [28, 29, 30, 31], vehicle crash test analysis, vehicle dynamics and dynamic deformation [32, 33, 34, 35, 36, 37, 38, 39, 40], video analysis [41, 42, 43], projection mapping [44,45], and photo scanning [46, 47, 48, 49]. All of these applications rely on pixel locations within photographs and video to create accurate measurements, projections, diagrams, point clouds and 3D models.

Camera lenses are curved in nature and introduce varying degrees of distortion in the resulting photographs. This lens distortion has been shown to have an impact on the accuracy of photogrammetric solutions [50,51]. When not accounted for, lens distortion can create less accurate photogrammetric results. While there are a number of methods for removing lens distortion from photographs, traditional methods rely on either having access to the camera, or knowing what camera and lens were used when the photograph was taken.

This paper presents two methods for removing lens distortion from photographs that do not have EXIF (Exchangeable image file format) data, such that camera and lens information can be determined. The first method presented is referred to as the straight-line method. This method utilizes linear objects within the photograph to determine and remove lens distortion. The second method presented is referred to as the point cloud method. This method utilizes a 3D point cloud and photogrammetric principles to solve for and remove lens distortion from the photographs. To evaluate the accuracy of these methods, the following three cameras were chosen.

1. Kodak EasyShare Z8612 IS
2. Olympus C-7070 Wide Zoom
3. Samsung ES15

These cameras were chosen because they are cameras with lens distortion profiles recognized by commercially available lens distortion removal software, and because they are known to have been used by law enforcement to document accident sites. To gain an understanding of the efficacy of these methods at removing lens

distortion and to compare the resulting photogrammetric solutions achieved in a real world setting, a study site was setup. This site was prepared in an intersection, and roadway markings were placed within the site to represent locations of evidence on the roadway. The intersection and surrounding landmarks were mapped using both a total station and a 3D laser scanner. Spray chalk was used on the roadway surface to represent evidence locations. These spray chalk locations were both photographed with all three cameras from multiple locations and separately mapped with the total station. A 3D diagram of the scene was processed using LiDAR data collected by both the total station and the 3D laser scanner and camera matching photogrammetry was then used to place the evidence within the 3D diagram of the scene. Photogrammetric placement of evidence from the following data sets was compared to the total station location of evidence to aid in evaluating the accuracy of the following lens distortion removal methods.

1. Distorted photographs (no lens distortion removed)
2. Distortion removed – library based software
3. Distortion removed – straight-line method
4. Distortion removed – point cloud method

Additionally, multiple locations of the three physical cameras were recorded by the total station. These locations represent the camera center of lens where the photographs were taken. The camera locations were then compared to the camera locations achieved with the photogrammetric solutions for the same four solution groups as listed above.

The amount of lens distortion, both present and removed, was also analyzed from a pixel location standpoint. For this process the lens distortion profiles achieved from both the straight-line method and the point cloud method were applied to a grid. Similarly, the traditional or software library based lens distortion profiles were also applied to a grid. Resulting pixel locations were then compared to an undistorted grid to gain an understanding of image pixel movement throughout each lens distortion profile.

Background

Pincushion and barrel distortion are the two most common types of symmetric radial lens distortion. Wavy or what is sometimes referred to as moustache distortion is a combination of both pincushion and barrel distortion (Figure 1).

There are other types of lens distortion and lens aberrations including fisheye, and decentering lens distortion [50]. While some software is capable of dealing with and solving for these types of distortion, for the purposes of this study, the symmetric radial distortion types referred to as barrel, pincushion and wavy are considered.

There are many types of software available for removing lens distortion from photographs. Table 1 is a sample of some of the most common software titles that can be used for lens distortion removal, including their capabilities and information or equipment required. There exist a number of photogrammetry based software titles that are capable of creating point clouds using multiple photographs.

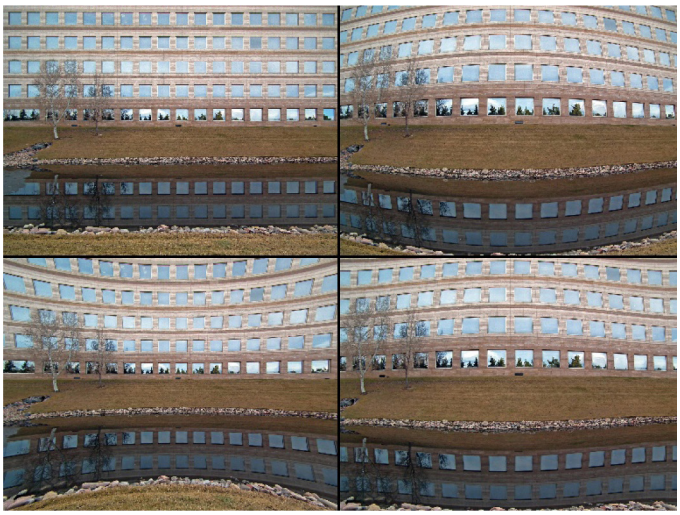

Figure 1. Lens distortion types – Top left: undistorted, Top Right: barrel distortion, bottom left: pincushion distortion, bottom right: wavy distortion.

Some of these titles are capable of automatically solving for lens distortion as well. This software list is not exhaustive.

Table 1. Sample list of software titles available for lens distortion correction.

Software	Version	Auto-(Library)	Lens Profile Needed	Camera Needed (Grid)	Point Cloud	Straight Line
ACDSee Pro/ Ultimate	10	X				
Adobe Lens Profile Creator	1.0.4			X		
Adobe Photoshop / Lightroom	2017	X				
DXO Viewpoint	2.5.17	X				
Hugin	2016.2.0	X	X	X		X
ImageMagick	7.0-3-4		X			
Nuke	10		X	X	X	X
PFTrack	2015.1.1		X	X	X	X
PTLens	9.0	X				

In general lens distortion can be grouped into automatic or library based and manual based distortion removal. Automatic distortion removal requires little input from the user and bases the distortion removal on a library of known lens profiles. A good example of this is PTLens. When a photograph is loaded into PTLens, the software automatically looks to the EXIF data which is stored within the metadata of digital photographs. This data can specify the camera make, model, lens, lens settings, and other parameters used when the photograph was taken. If the camera lens is recognized within the software library of known lenses, the software automatically removes the distortion without additional input from the user. GoPro is another example of this. While their cameras are known to have more of a fisheye lens distortion type, they have responded to the desire for users to remove lens distortion by releasing GoPro Studio. This free software that automatically recognizes lens distortion amounts based on EXIF data and gives users the ability to remove the distortion from their footage.

It is worth noting that many camera manufacturers are releasing newer camera models that can automatically correct for the lens distortion within the firmware, prior to saving the photograph to memory. Depending on the model, this feature is either built in or given to users as an option. Another method utilized by some software titles is the option of calibrating a camera to be used for photogrammetry. This process is typically described in detail by the software manual, and can vary per software title.

Some multi-view photogrammetry or photo-scanning software titles capable of generating 3D point cloud data have the ability to automatically remove lens distortion during the point cloud generation process [52]. This can be dependent on the amount of lens distortion present, and may only correct for lens distortion within the point cloud solution, and not the individual photographs.

Manual distortion removal typically involves either having access to the lens profiles such that they can be manually entered into the software, or having the camera and camera lens available to photograph grid patterns. Adobe Lens Profile Creator is a good example of this type of software. It allows users with access to cameras used to create the photographs or video, to remove lens distortion by taking a series of photographs or video images of a specific grid. The software then analyzes the grid to determine the amount of lens distortion present and creates lens distortion profiles that allow the user to remove the lens distortion.

Methodology

Cameras

To test the effectiveness of both the straight-line method, as well as the point cloud method, three cameras with known lens distortion parameters were chosen. The three cameras all fall into the consumer-grade, point-and-shoot category of digital cameras, and are all known to have been used by law enforcement for photographing vehicle accident scene evidence (Table 2), (Figure 2).

Table 2. A comparison of cameras used in the study.

Camera	Resolution	Mega Pixels	Sensor Type	Sensor Size (mm)	Focal Length (35 mm eq.)
Kodak Z8612	3264 x 2448	8.1	CCD	5.8 x 4.3	36
Olympus C-7070WZ	3072 x 2304	7.1	CCD	7.2 x 5.3	27
Samsung ES15	3648 x 2736	10.2	CCD	6.2 x 4.6	35

Figure 2. Cameras used in the study. From left to right: Kodak Z8612, Samsung ES15, Olympus C7070WZ.

The widest field-of-view setting for digital point-and-shoot cameras is typically the default setting when the camera is turned on. This field-of-view is also well suited for photographing scenes. For these reasons, and because it has been the authors' experience that these settings are most commonly used in documenting vehicle accident scenes, this was the setting chosen for the cameras when documenting the study site. It is worth noting that the widest field of view typically contains higher amounts of lens distortion within the photograph.

Physical Study Site Layout and Documentation

For the purpose of this paper the intersection of two four lane divided roadways was chosen as a test study site. This intersection was chosen because it featured a number of vertical and straight-line features that could be photographed and used as a method for removing distortion from the photographs. The intersection was mapped using a Nikon Nivo 3M three second reflectorless total station and a FARO Focus 3D X 330 laser scanner (Figure3).

Figure 3. Test study site being mapped with a 3D laser scanner and a reflectorless total station.

LiDAR data from the total station and from the 3D laser scan data was then processed and aligned to create az 3D scene diagram of the intersection (Figure 4). This scene diagram represents data collected sometime after a vehicle accident, where evidence such as tire marks, vehicle debris and points of rest (POR) for the vehicles would no longer be visible at the accident site.

Figure 4. LiDAR data of the scene mapping. The color point cloud data is from the 3D laser scanner and black line work is from LiDAR data collected with the total station.

The same study site was revisited at a later point in time, and markings were laid out with orange spray chalk so that they would be visible within photographs (Figure 5).

Figure 5. Orange spray chalk, representing evidence on the roadway surface, being recorded with a total station.

The location of these markings were then recorded using a total station so that the recorded physical locations of the spray chalk markings could be compared to the virtual locations of the markings as determined by the photogrammetry solutions. Common points that were previously mapped were mapped again in this data set, so that this data could be aligned to the previous LiDAR data collected at the scene. This data was aligned, kept separate from the rest of the scene mapping, and used as a baseline for comparing photogrammetry solutions of the spray chalk mark locations. Figure 6 is a diagram comprising the study site mapping with specific spray chalk markings and camera locations labeled.

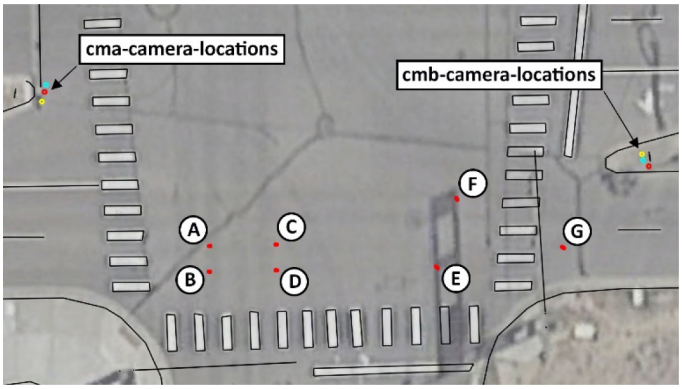

Figure 6. Diagram of the study site with labels for spray chalk markings, and camera photograph locations (cma and cmb).

The three cameras chosen for the study were then used to photograph the orange spray chalk markings from multiple vantages (Figure 7). The camera locations were also mapped using a total station, so that the physical location of the cameras within the study scene could be compared virtual camera locations resulting from the varying photogrammetry solutions. This data can be found in the analysis and results section (Figure 19).

Prior to removing lens distortion from the photographs, camera match photogrammetry was used to establish a baseline for physical site study comparisons. This was done for photograph sets taken with each of the three cameras. Due to the distortion within the photographs these camera matches did not align well with the total station and 3D laser scanner data in all areas of the photograph, and the photogrammetry solutions were achieved in a best-fit manner. The spray markings were then located within these matches such that their 3D locations could be compared to corresponding total station data of the same spray markings.

Figure 7. The Three study cameras on location at the test study site. From left to right: Samsung ES15, Olympus C7070WZ, Kodak Z8612.

The six photographs that were used for this study as well as the resulting photogrammetry solutions for each of the distorted and undistorted photographs sets are available in Appendix A.

Automatic, Library-Based Method

PTLens is a software title designed specifically for removing lens distortion from photographs. PTLens was chosen as a more traditional method of lens distortion removal and used to establish a comparison for both the straight-line and the point cloud lens distortion removal methods. Lens distortion profiles for all three of the study cameras are part of the PTLens library or database of lens profiles. By default, PTLens crops out the curved portions of a photograph that cannot be contained within a rectangular shape. This does not typically present an issue for photogrammetry, as without distortion, the camera solution can be solved for regardless of the overall dimensions of the photograph. Our study purposed to compare both real world photogrammetry results as well as pixel movement results between the different lens distortion removal methods. In effort to avoid pixel shift from cropping, it was necessary to obtain the entire undistorted photograph without cropping. The PTLens software author was gracious to provide us with the lens distortion coefficients for each of the cameras from the PTLens database (Table 3).

Table 3. Coefficients provided by the author of PTLens.

	Olympus	Samsung	Kodak
a	0	0.0245	0.0301
b	-0.0047	-0.0585	-0.0733
c	-0.0256	0	0

The following equation with *a*, *b,* and *c* coefficients can be used in removing lens distortion, where *r'* represents a distorted pixel location and *r* an undistorted pixel location. *r* and *r'* refer to the normalized radius of an image pixel. Parameter *d* is set to be 1-(*a*+*b*+*c*) which resolves into *r* = *r'* at *r* = 1. (This means the upper and lower center pixel of the image will not shift.)

$$r' = ar^4 + br^3 + cr^2 + dr$$ [53]

These coefficients were then run through ImageMagick to obtain an uncropped and undistorted version of the photograph. Using this method, lens distortion was removed from the six photographs used for analysis (Three cameras and two locations).

After applying the corrections, the library-based undistorted photographs were used in camera matching photogrammetry. The scene total station mapping data and 3D laser scan data were used to establish a 3D environment of the study site. A virtual camera was then created and the straight-line undistorted photograph was set as the background image within the virtual camera. The position, rotation and field of view were then manually adjusted until the environment aligned with the photograph. This camera matching process was accomplished using Autodesk 3D Studio Max 2016 (Figure 8).

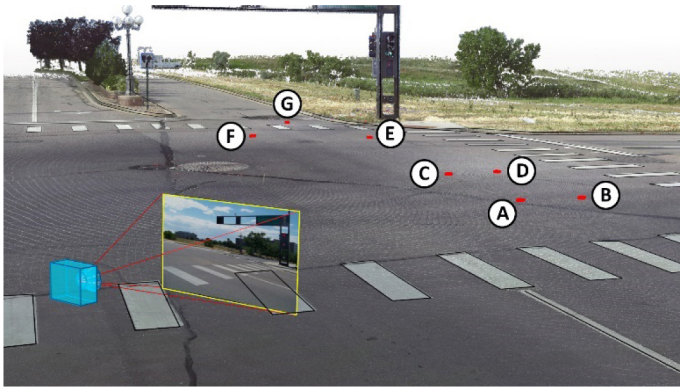

Figure 8. Camera match photogrammetry showing the location of the virtual camera within the 3D point cloud environment, and the labeled spray mark evidence on the ground surface. Photograph taken with the Kodak Z8612

The reference spray chalk marks within the photographs were then traced onto ground surface data generated using the total station and laser point cloud data so that the photogrammetry solution using the straight-line methodology for lens distortion removal could be compared with to the scene total station data of the reference spray chalk marks.

Straight-Line Method

When the camera lens is not known, the straight-line method can be used as an effective method for removing lens distortion and whereby improving photogrammetric solutions. This method is similar to the manual method of photographing a grid for software analysis in that it relies on linear features within the photograph to determine and solve for lens distortion. For this reason, not all photographs are well suited for this method. Some examples of linear features that can be used for this method include: vehicle trailers, utility posts, street lights, stop lights, buildings, bridges, signage and other man-made structures. Figure 9, is a photograph of a street light and building that were used for analysis in this study. This photograph was taken with the Kodak Z8612 camera in its default or widest field of view setting.

This straight-line method is achievable in other software titles as well, but for the purposes of this study PFTrack by Pixel Farm was used. Using an undistort node, curved lines were plotted to describe the straight lines as visible in Figure 9, so that lens distortion could be solved for and removed. The resulting parameters for lens distortion removal can be saved and then utilized on other photographs or video frames. For comparison purposes, after achieving a solution using the photograph as shown in Figure 9, the distortion parameters were applied to an idealized grid to gain an understanding of the amount and direction of pixel movement (Figure 10).

Figure 9. Photograph showing example of several linear objects used for removing lens distortion. This photograph was taken with the Kodak Z8612.

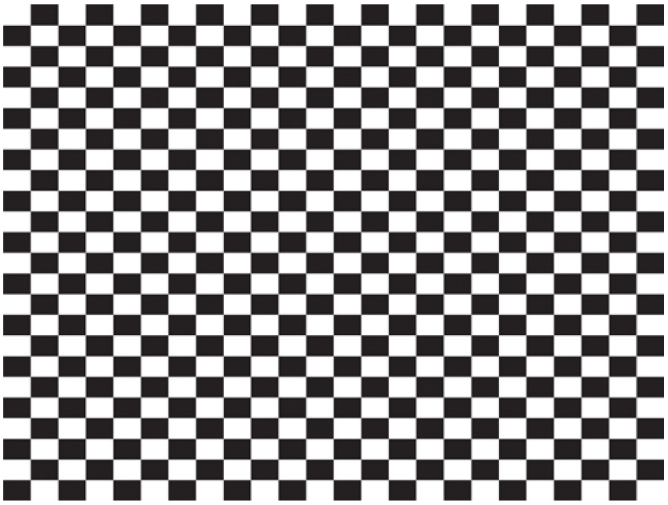

Figure 10. Idealized grid used in pixel movement analysis

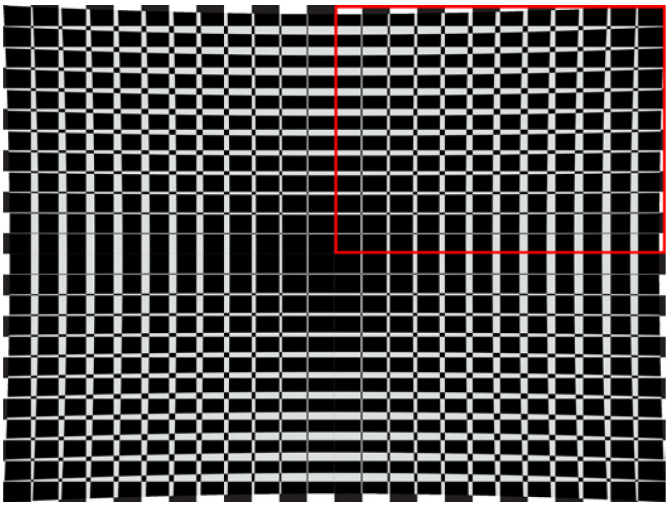

Figure 11. Idealized grid image with a difference overlay of the same grid with the Olympus C7070WZ straight-line lens distortion correction applied. Horizontal and vertical white areas indicate amount and location of pixel movement. The red area is shown larger in Figure 12.

Figures 11 and 12 show a difference overlay of both the original image of the grid and the same grid after applying the distortion removal. The width of the white lines represents the amount of pixel movement. In areas where the white lines are small or not visible, there is no distortion. Figure 11 shows the entire image overlay, and Figure 12 shows only the top right quarter or quadrant of the image.

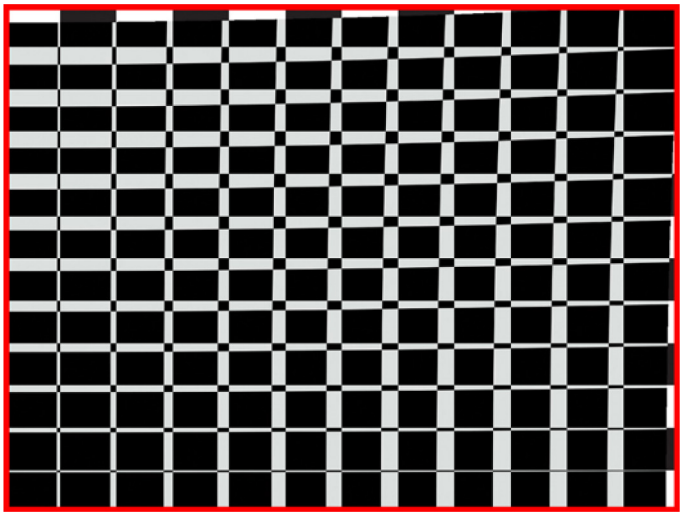

Figure 12. The top right quarter of Figure 11. This idealized grid image has a difference overlay of the same grid with the Olympus C7070WZ straight-line lens distortion correction applied. Horizontal and vertical white areas indicate amount and location of pixel movement.

The straight-line correction method was used to determine lens distortion for all three study cameras. After applying the corrections, the straight-line undistorted photographs were used in camera matching photogrammetry. This process was identical to the camera matching process described within the automatic library-based method (Figure 8).

Care should be used when selecting straight-line objects within photographs. Wooden telephone poles are sometimes warped, pre-stressed concrete structures can have some curvature to them, and other features that might typically be assumed to be straight, may have some curvature to them that would prevent them from being useful as straight-line objects in this method. The straight-line method does involve the manual tracing of straight objects. This tracing, the number of lines used, the length of the lines, and the areas within the photograph that these objects are located can all have an effect on results. For these reason, hard lined objects with easily distinguishable edges that extend throughout more of the photograph are preferable.

Point Cloud Method

When the camera lens is not known, the point cloud method can also be used to remove lens distortion and improve photogrammetric solutions. This method requires a three dimensional point cloud with sufficient density to accurately represent discrete points visible within the photograph. In the process of solving for lens distortion, this method also solves for the location, orientation, and field of view of the camera. As an additional benefit, the resulting virtual camera created during this photogrammetric solution, can be exported and further utilized in other software.

While other software titles may be capable of performing these calculations, for the purpose of this study the authors used PFTrack by Pixel Farm. After selecting the photograph for analysis and importing it, 3D point cloud data of the study site was also imported in a “x y z r g b” space-delimited file with the intensity values removed. This point cloud data was imported onto a survey solver node. Common points or trackers, were then selected within the photograph as well as the point cloud. These points were then analyzed by the software such that a camera positon could be determined (Figure 13).

Figure 13. Point cloud data visible within PFTrack. Points chosen as common points or trackers are visible accompanied with blue text to the right of the point. This image shows 9 common points chosen for analysis.

The software also gives the user ability to solve for radial lens distortion, whereby improving the overall photogrammetric alignment or automated camera match solution. The resulting lens distortion parameters can then be saved and applied to additional photographs or video frames.

Care should be taken when selecting point cloud data points that represent the points within the photographs. Due to the number of points within a point cloud, it is easy to accidently select a point that is not in the correct location. Rotating around selected points and verifying precision of the selection as well as verifying that point cloud density is sufficient to describe the corresponding point is important for achieving accurate results. The authors have also experienced a greater accuracy in point selection by using grayscale, reflectivity based point cloud data over the RGB photograph overlay data. When applying this method, it is recommended that reflectivity based point cloud data is used for point cloud selections or trackers whenever possible.

Analysis/Results

Straight-Line Method: Radial Pixel Movement

Radial pixel movement was calculated for each of the lens distortion removal methods starting in the center of the image and moving diagonally to a corner of the image. This was done by creating three 24x24 idealized checkerboard grids with the same dimensions as photographs. The photographs from all three cameras had a dimensional ratio of 4:3 and so the grid consisted of 4x3 proportioned rectangles, such that thirteen intersecting corner grid points could be calculated from the center to the diagonal corner of the image (Figure 14).

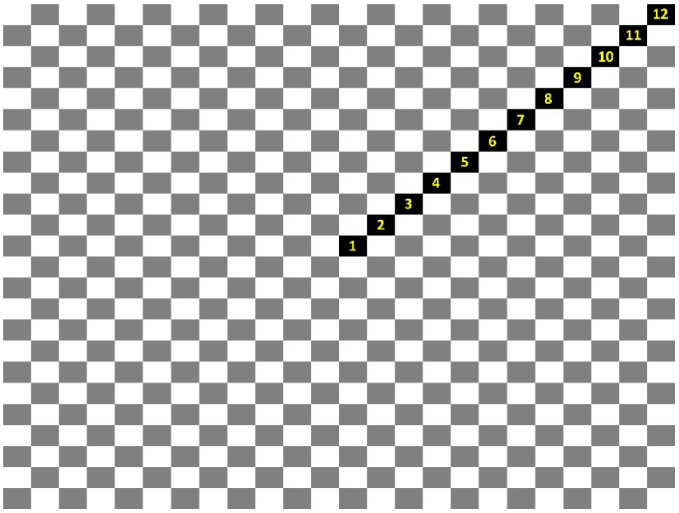

Figure 14. Idealized, checkerboard grid with twelve 4x3 rectangles specified for tracking pixel movement between lens distortion solutions.

This grid was then distorted using the PTLens coefficients. Before pixel movement analysis, the grids were aligned to have the same overall dimensions as the original photographs, eliminating pixel movement differences resulting from the scaling of images.

To analyze the amount of radial pixel movement, the height and width for each of the 12 grid squares was measured. Table 4 contains the measurements from the Olympus formatted grid prior to using the lens profiles for distortion. The distance column consistently grows by 160 pixels per row, as there is no distortion. The percentage for each of the 13 locations (0-12) corresponds to the percentage diagonally from the center to the corner of the photograph as shown in Figure 14. These percentages also correlate to the data points on the radial pixel movement probability plots (Figures 15, 17).

This same process was then applied using the lens distortion solutions for both the straight-line and the point cloud methods. This was done separately for all three of the cameras and for both of the camera locations. After applying the corrections for each data set to the grid, the same measurements for width and height were taken so that the radial, or diagonal distance across each section of the grid could be analyzed. Table 5 is an example of the individual height and width grid measurements taken after the library-based PTLens corrections were applied to the grid. The difference column shows the diagonal distance difference for each of the 13 data points as compared to the undistorted grid point locations.

Table 4. Undistorted grid measurements (Olympus)

Olympus: Undistorted				
	Width	**Height**	**Dist.**	**%**
0	0	0	0	0
1	128	96	160	8
2	128	96	320	17
3	128	96	480	25
4	128	96	640	33
5	128	96	800	42
6	128	96	960	50
7	128	96	1120	58
8	128	96	1280	67
9	128	96	1440	75
10	128	96	1600	83
11	128	96	1760	92
12	128	96	1920	100
Sum	1536	1152		

Table 5. Grid measurements with PTLens correction applied (Olympus)

Olympus: PTLens				
	Width	**Height**	**Dist.**	**Diff.**
0	0	0	0	0
1	121	91	151	9
2	122	92	304	16
3	124	92	459	21
4	124	93	614	26
5	125	94	770	30
6	127	95	929	31
7	128	96	1089	31
8	129	97	1250	30
9	131	99	1414	26
10	133	99	1580	20
11	135	102	1749	11
12	137	102	1920	0
Sum	1536	1152		252

The resulting pixel movements from the straight-line method were then compared to pixel movement within the PTLens lens distortion models for each camera from two different camera locations. Table 6 contains the measurements for the width and height of each of the 13 grid points after applying the straight-line method solution from the Olympus camera at the CMB location. The difference column shows the diagonal distance difference from the undistorted grid point locations.

Table 6. Grid measurements using Straight-Line Method (Olympus CMB)

Olympus: Straight-line CMB				
	Width	Height	Dist.	Diff.
0	0	0	0	0
1	122	92	153	7
2	123	92	306	14
3	123	92	460	20
4	124	93	615	25
5	125	94	771	29
6	125	94	928	32
7	128	96	1088	32
8	129	96	1249	31
9	130	98	1411	29
10	133	100	1578	22
11	135	101	1746	14
12	139	104	1920	0
Sum	1536	1152		255

Using the PTLens profiles as a baseline and with respect to original pixel location, the straight-line method was shown to improve pixel location by an average of 82% overall. A maximum improvement of 99% resulted from the Olympus CMB dataset, as these grid point locations moved 99% closer to the Olympus PT Lens solution than the uncorrected grid (Table 6). Likewise, a minimum improvement of 34% resulted from the Samsung CMA grid point locations, as these points moved 34% closer to the Olympus PT Lens solution than the uncorrected grid (Appendix B). Figure 15 is a probability plot showing the amount of pixel movement over percentages of the photograph starting from the center and moving diagonally to the corner.

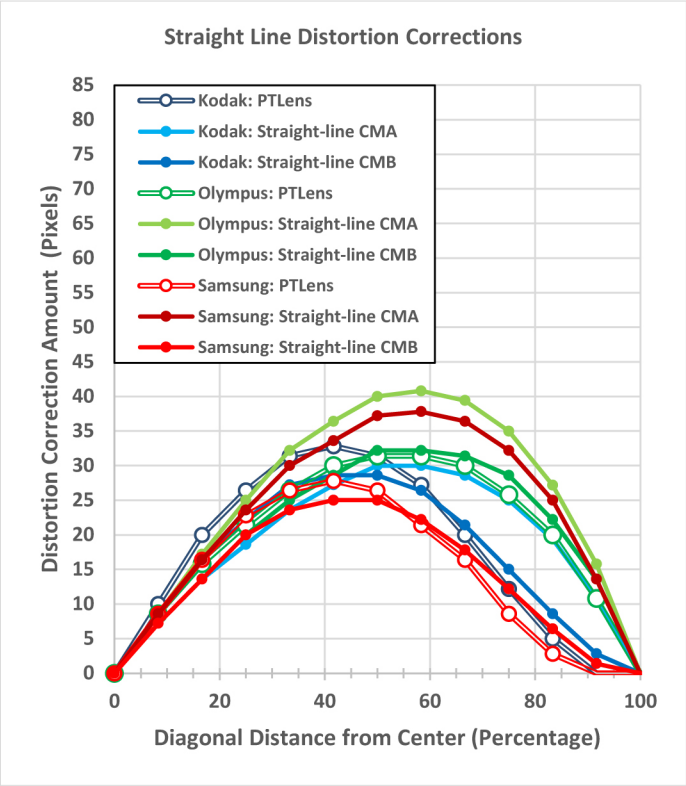

Figure 15. Radial pixel movement over percentage of photographs from center diagonally to the corner, for all three cameras in both camera match locations (CMA, CMB).

The pixel measurements for all images using the straight-line and point cloud methods as well as additional probability plots of this data are included in Appendix B.

Straight-Line Method: Photogrammetry

In addition to the radial pixel movement analysis, lens distortion removal accuracy for the straight-line method was also analyzed using camera match photogrammetry. In this analysis, photogrammetry was used to determine the three-dimensional location of roadway spray chalk marks visible within the photographs. The resulting photogrammetry based locations were then compared to corresponding LiDAR based total station data for the spray chalk marks. Overall the straight-line method was found to be an average of 9.9 centimeters from the corresponding LiDAR points. Table 7 contains the LiDAR based locations for the spray chalk, as well as the corresponding spray chalk locations determined through photogrammetry using the Kodak CMA photograph without distortion correction, the Kodak CMA photograph with lens distortion corrections from PTLens, and the Kodak CMA photograph with straight-line method distortion corrections applied. The distance from LiDAR is a total distance in cm, derived from the X, Y, and Z locations.

Table 7. Spray Chalk Locations from total station mapping (LiDAR), and photogrammetry based locations for the Kodak CMA camera, for the uncorrected distortion image, the PTLens distortion corrected image and the straight-line distortion corrected image.

Spray Chalk Locations (LiDAR)				
	X	Y	Z	
A	-282.29	252.11	5994.43	
B	-348.53	244.20	5994.11	
C	-256.33	84.54	5997.43	
D	-322.01	74.98	5996.71	
Kodak - CMA - Uncorrected Distortion				**Dist. From LiDAR (cm)**
	X	Y	Z	
A	-279.67	251.11	5994.30	7.1
B	-345.53	245.56	5993.87	8.4
C	-256.93	73.46	5997.39	28.2
D	-319.00	68.50	5996.69	18.2
			Average	**15.5**
Kodak - CMA - PTLens				**Dist. From LiDAR (cm)**
	X	Y	Z	
A	-284.72	251.31	5994.30	6.5
B	-350.3	243.85	5993.85	4.6
C	-256.95	82.16	5997.29	6.3
D	-322.31	73.66	5996.59	3.4
			Average	**5.2**
Kodak - CMA - Straight-Line				**Dist. From LiDAR (cm)**
	X	Y	Z	
A	-280.02	255.04	5994.20	9.4
B	-346.66	246.44	5993.84	7.4
C	-253.16	86.06	5997.29	8.9
D	-319.75	73.25	5996.63	7.2
			Average	**8.3**

Figure 16 shows average distances for the straight-line method and includes data from all three cameras at two different locations for a total of six straight-line data sets. Figure 16 also compares these distances to the corresponding photogrammetry data sets resulting from the photographs without lens distortion correction and the PTLens corrected photographs.

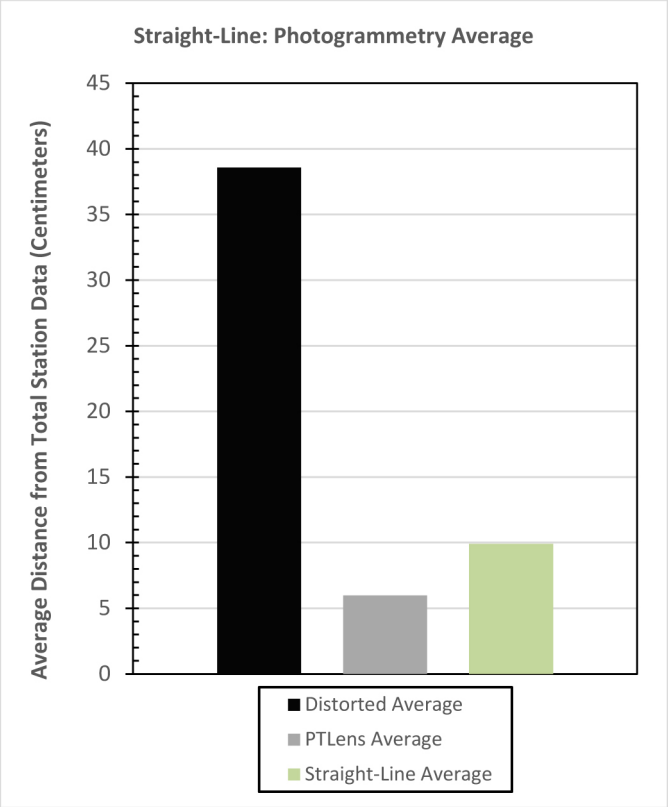

Figure 16. Average distance for spray chalk points located through photogrammetry from total station spray chalk points. Corresponding spray chalk distances for both the uncorrected or distorted photographs and the PTLens corrected photograph data sets are included with the straight-line data set for comparison.

Point Cloud Method: Radial Pixel Movement

The same idealized, checkerboard grid process as described in the straight-line method was utilized to compare pixel movement within the point cloud method for lens distortion removal. These data sets were again compared to distortion removal models as defined by the PTLens coefficients. This comparison was made for both photograph sets taken with each of the three study cameras for a total of six data sets. Using the PTLens profiles as a baseline and with respect to original pixel location, the point cloud method was shown to improve pixel location by an average of 40% overall. A maximum improvement of 66% resulted from the Olympus CMA dataset, as these straight-line grid point locations moved 66% closer to the PTLens solution than the uncorrected grid (Appendix B). Likewise, a minimum improvement of 10% resulted from the Samsung CMB dataset, as these grid point locations moved 10% closer to the PTLens solution than the uncorrected grid (Appendix B). Figure 17 is a probability plot showing the amount of pixel movement over percentages of the photograph starting from the center and moving diagonally to the corner.

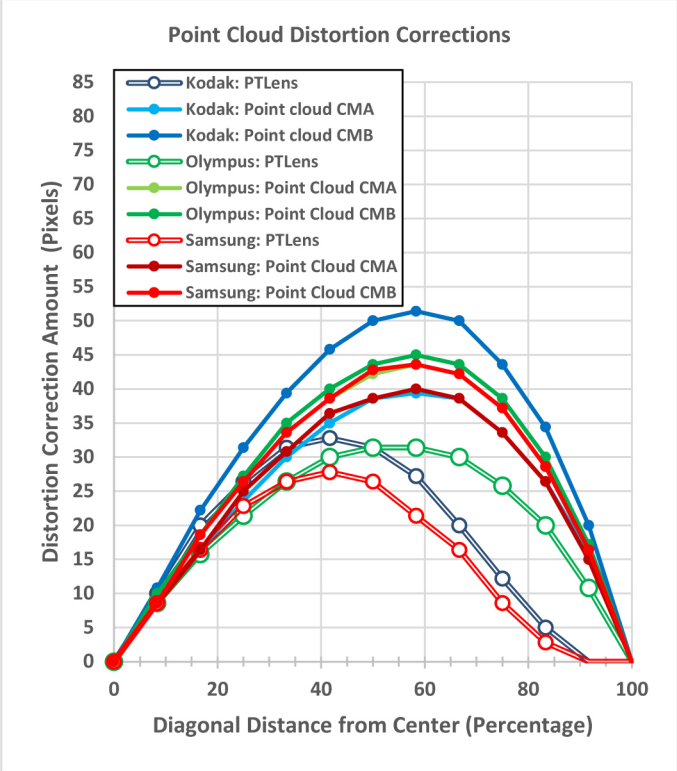

Figure 17. Radial pixel movement over percentage of photographs from center diagonally to corner for all three cameras in two separate camera match locations (CMA, CMB).

Tables for radial pixel movement for each of the data sets, as well as probability plots comparing pixel movement for both the straight-line and point cloud methods to the PTLens solution is available in Appendix B.

Point Cloud Method: Photogrammetry

Distortion removal accuracy for the point cloud method was also compared using camera match photogrammetry. Spray chalk marks from the point cloud photogrammetry solutions were compared to corresponding spray chalk marks as recorded with the total station. Unlike the straight-line method where adjustments were made to the virtual camera until an overlay was achieved, this method automatically generated camera positions within the software photogrammetry solution while solving for lens distortion. The virtual camera positions and characteristics for all three cameras at the CMA position were not adjusted and only minor adjustments were made to the virtual cameras at the CMB positions. Overall the point cloud method was found to be an average of 11.3 centimeters from the corresponding LiDAR points. Figure 18 shows the average photogrammetry based distances for the point cloud method from total station (LiDAR) data and compares this to corresponding photogrammetry based data from both the uncorrected or distorted photographs and the PTLens corrected photographs.

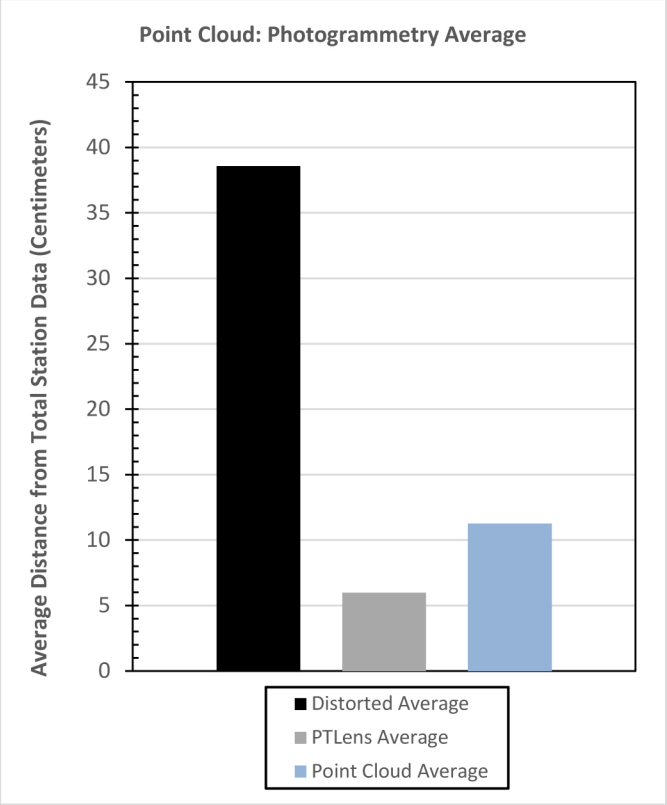

Figure 18. Distance for spray chalk points located through photogrammetry from total station spray chalk points. Spray chalk distances for uncorrected or distorted and PTLens corrected sets are included with the point cloud data set for comparison.

Additional graphs comparing photogrammetry based spray paint locations to corresponding LiDAR based locations for both the straight-line and point cloud methods of lens distortion removal, are available by camera in Appendix B.

Camera Locations

Camera locations that were documented with the total station were also compared to the photogrammetry data set virtual camera locations. The photogrammetry solutions with the distorted or uncorrected photographs were an average of 11.7 centimeters from the total station recorded physical camera locations. Virtual cameras from the PTLens distortion removal photogrammetry solutions were an average of 4.3 centimeters from the recorded physical camera locations. Virtual cameras from the straight-line distortion removal photogrammetry solutions were an average of 4.0 centimeters from the recorded physical camera locations. Virtual cameras from the **p**oint cloud lens distortion removal were an average of 4.1 centimeters from the recorded physical camera locations (Figure 19).

The physical camera locations were documented with the total station at the center of lens for each camera location. The offset from the camera image sensor to the lens may account for some of the distance between the virtual camera locations and the physical camera locations as recorded by the total station.

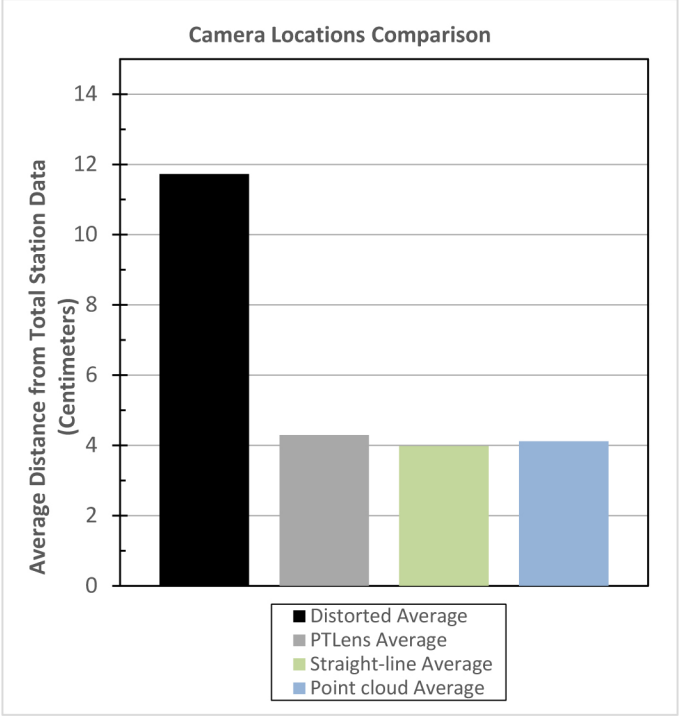

Figure 19. Virtual camera locations from photogrammetry solutions distance comparison from total station recorded camera locations.

Conclusions

Both the straight-line method as well as the point cloud method for removing lens distortion show significant improvement over the original distorted photograph when compared to accepted, library-based software used for lens distortion removal. These improvements are visible both in the pixel location analysis as well as the real world study for analyzing the impact on photogrammetric results. The authors utilized camera-matching photogrammetry to illustrate the benefit of these lens distortion removal methods on photogrammetry. Lens distortion has adverse effects on photogrammetry solutions in general, and the benefit of these lens distortion removal methods is not limited to a specific photogrammetry method or software title. There are numerous photogrammetry software titles on the market and similar results can be expected within these software titles, after employing these methods for lens distortion removal. The authors have found these methods useful for removing distortion from both photographs and video and believe technological advancements in both the software and hardware development will continue to improve results for both of these methods of lens distortion removal beyond those presented within this paper.

References

1. Wolf, P., Dewitt, B., and Wilkinson, B., *Elements of Photogrammetry with Application in GIS 4/E*. 4th ed.New York: McGraw-Hill Professional Publishing, 2014.
2. Fenton, S. and Kerr, R., "Accident Scene Diagramming Using New Photogrammetric Technique," SAE Technical Paper 970944, 1997, doi:10.4271/970944.

3. Neale, W., Fenton, S., McFadden, S., and Rose, N., "A Video Tracking Photogrammetry Technique to Survey Roadways for Accident Reconstruction," SAE Technical Paper 2004-01-1221, 2004, doi:10.4271/2004-01-1221.
4. Day, T. and Hargens, R., "A Personal Computer Program for Drawing Accident Sites," SAE Technical Paper 880068, 1988, doi:10.4271/880068.
5. Coleman, C., Tandy, D., Colborn, J., and Ault, N., "Applying Camera Matching Methods to Laser Scanned Three Dimensional Scene Data with Comparisons to Other Methods," SAE Technical Paper 2015-01-1416, 2015, doi:10.4271/2015-01-1416.
6. Rudny, D. and Sallmann, D., "The Use of Electronic Survey Equipment in the Creation of Accident Scene Diagrams," SAE Technical Paper 950361, 1995, doi:10.4271/950361.
7. Niederer, P., Birchler, B., Mesqui, F., and Lehareinger, Y., "Computer Assisted Single-View Photogrammetry for Accident Scene Documentation," SAE Technical Paper 850067, 1985, doi:10.4271/850067.
8. Breen, K. and Anderson, C., "The Application of Photogrammetry to Accident Reconstruction," SAE Technical Paper 861422, 1986, doi:10.4271/861422.
9. Kinney, J. and Magedanz, B., "TRANS4 - A Traffic Accident Photogrammetric System, Description of the System and Its Inherent Errors," SAE Technical Paper 861417, 1986, doi:10.4271/861417.
10. Grimes, W., Culley, C., and Cromack, J., "Field Application of Photogrammetric Analysis Techniques: Applications of the FOTOGRAM Program," SAE Technical Paper 861418, 1986, doi:10.4271/861418.
11. Tumbas, N., Kinney, J., and Smith, G., "Photogrammetry and Accident Reconstruction: Experimental Results," SAE Technical Paper 940925, 1994, doi:10.4271/940925.
12. Pepe, M., Sobek, J., and Huett, G., "Three Dimensional Computerized Photogrammetry and its Application to Accident Reconstruction," SAE Technical Paper 890739, 1989, doi:10.4271/890739.
13. Pepe, M., Sobek, J., and Zimmerman, D., "Accuracy of Three-Dimensional Photogrammetry as Established by Controlled Field Tests," SAE Technical Paper 930662, 1993, doi:10.4271/930662.
14. Pepe, M., Grayson, E., and McClary, A., "Digital Rectification of Reconstruction Photographs," SAE Technical Paper 961049, 1996, doi:10.4271/961049.
15. Main, B. and Knopf, E., "A New Application of Camera Reverse Projection in Reconstructing Old Accidents," SAE Technical Paper 950357, 1995, doi:10.4271/950357.
16. Randles, B., Jones, B., Welcher, J., Szabo, T., "The Accuracy of Photogrammetry vs. Hands-on Measurement Techniques used in Accident Reconstruction," SAE Technical Paper 2010-01-0065, 2010, doi:10.4271/2010-01-0065.
17. DeChant, L. and Kinney, J., "A Close-Range Photogrammetric Solution Working with Zoomed Images from Digital Cameras," SAE Technical Paper 2012-01-0612, 2012, doi:10.4271/2012-01-0612.
18. Hovey, C. and Toglia, A., "Four-Point Planar Homography Algorithm for Rectification Photogrammetry: Development and Applications," SAE Technical Paper 2013-01-0780, 2013, doi:10.4271/2013-01-0780.
19. Campbell, A. and Friedrich, R., "Adapting Three- Dimensional Animation Software for Photo grammetry Calculations," SAE Technical Paper 930904, 1993, doi:10.4271/930904.
20. Callahan, M., LeBlanc, B., Vreeland, R., and Bretting, G., "Close-Range Photogrammetry with Laser Scan Point Clouds," SAE Technical Paper 2012-01-0607, 2012, doi:10.4271/2012-01-0607.
21. Wester-Ebbinghaus, W. and Wezel, U., "Photogrammetric Deformation Measurement of Crash Vehicles," SAE Technical Paper 860207, 1986, doi:10.4271/860207.
22. Gillen, L., "Photogrammetric Mapping of Vehicle Deformations," SAE Technical Paper 861421, 1986, doi:10.4271/861421.
23. Fenton, S., Neale, W., Rose, N., and Hughes, C., "Determining Crash Data Using Camera Matching Photogrammetric Technique," SAE Technical Paper 2001-01-3313, 2001, doi:10.4271/2001-01-3313.
24. CRASH TEST ANALYSIS
25. Rentschler, W. and Uffenkamp, V., "Digital Photogrammetry in Analysis of Crash Tests," SAE Technical Paper 1999-01-0081, 1999, doi:10.4271/1999-01-0081.
26. Behring, D., Thesing, J., Becker, H., and Zobel, R., "Optical Coordinate Measuring Techniques for the Determination and Visualization of 3D Displacements in Crash Investigations," SAE Technical Paper 2003-01-0891, 2003, doi:10.4271/2003-01-0891.
27. O'Shields, L., Kress, T., Hungerford, J., and Aikens, C., "Determination and Verification of Equivalent Barrier Speeds (EBS) Using PhotoModeler as a Measurement Tool," SAE Technical Paper 2004-01-1208, 2004, doi:10.4271/2004-01-1208.
28. Switzer, D. and Candrlic, T., "Factors Affecting the Accuracy of Non-Metric Analytical 3-D Photogrammetry, Using PhotoModeler," SAE Technical Paper 1999-01-0451, 1999, doi:10.4271/1999-01-0451.
29. Peck, L. and Cheng, M., "The Accuracy of an Optimized, Practical Close-Range Photogrammetry Method for Vehicular Modeling," *SAE Int. J. Trans. Safety* 4(2):245–266, 2016, doi:10.4271/2016-01-1462.
30. Erickson, M., Bauer, J., and Hayes, W., "The Accuracy of Photo-Based Three-Dimensional Scanning for Collision Reconstruction Using 123D Catch," SAE Technical Paper 2013-01-0784, 2013, doi:10.4271/2013-01-0784.
31. Ball, J., Danaher, D., and Ziernicki, R., "A Method for Determining and Presenting Driver Visibility in Commercial Vehicles," SAE Technical Paper 2007-01-4232, 2007, doi:10.4271/2007-01-4232.
32. Chou, C., McCoy, R., Le, J., Fenton, S., "Image Analysis of Rollover Crash Tests Using Photogrammetry," SAE Technical Paper 2006-01-0723, 2006, doi:10.4271/2006-01-0723.

33. Rose, N., Neale, W., Fenton, S., Hessel, D., "A Method to Quantify Vehicle Dynamics and Deformation for Vehicle Rollover Tests Using Camera-Matching Video Analysis," *SAE Int. J. Passeng. Cars - Mech. Syst.* 1(1):301–317, 2009, doi:10.4271/2008-01-0350.
34. Chou, C., Hu, J., Yang, K., and King, A., "A Method for Determining the Vehicle-to-Ground Contact Load during Laboratory-based Rollover Tests," *SAE Int. J. Passeng. Cars* - Mech. Syst.1(1):318–325, 2009, doi:10.4271/2008-01-0351.
35. Smith, G. and Allsop, D., "A Case Comparison of Single-Image Photogrammetry Methods," SAE Technical Paper 890737, 1989, doi:10.4271/890737.
36. Byers, L. and Slon, C., "A Method for Improving the Accuracy of Standard Stereo Photogrammetry When Using Small Subtended Angles," SAE Technical Paper 2005-01-0751, 2005, doi:10.4271/2005-01-0751.
37. McClenathan, R., Nakhla, S., McCoy, R., and Chou, C., "Use of Photogrammetry in Extracting 3D Structural Deformation/ Dummy Occupant Movement Time History During Vehicle Crashes," SAE Technical Paper 2005-01-0740, 2005, doi:10.4271/2005-01-0740.
38. Kullgren, A., Lie, A., and Tingvall, C., "The Use of Photogrammetry and Video Films in the Evaluation of Passenger Compartment Measurement and Occupant-Vehicle Contacts," SAE Technical Paper 950239, 1995, doi:10.4271/950239.
39. Karvelis, A., Rogers, M., Anderson, C., and Liubinskas, A., "Computer-Aided 3-D Surface Reconstruction During High Speed Crush Events," SAE Technical Paper 910320, 1991, doi:10.4271/910320.
40. Harvin, S., O'Brien-Mitchell, B., Dwoinen, A., Nassoiy, C., "Evaluation of Dynamic Roof Deformation in Rollover Crash Tests," *SAE Int. J. Passeng. Cars – Mech. Syst.* 4(1):807–829, 2011, doi:10.4271/2011-01-1093.
41. Massa, D., "Using Computer Reverse Projection Photogrammetry to Analyze an Animation," SAE Technical Paper 1999-01-0093, 1999, doi:10.4271/1999-01-0093.
42. Alden, A., Mayer, B., Mcgowen, P., Sherony, R., "Animal-Vehicle Encounter Naturalistic Driving Data Collection and Photogrammetric Analysis," SAE Technical Paper 2016-01-0124, 2016, doi:10.4271/2016-01-0124.
43. Neale, W., Hessel, D., and Koch, D., "Determining Position and Speed through Pixel Tracking and 2D Coordinate Transformation in a 3D Environment," SAE Technical Paper 2016-01-1478, 2016, doi:10.4271/2016-01-1478.
44. Neale, W., Marr, J., and Hessel, D., "Nighttime Videographic Projection Mapping to Generate Photo-Realistic Simulation Environments," SAE Technical Paper 2016-01-1415, 2016, doi:10.4271/2016-01-1415.
45. Neale, W., Marr, J., and Hessel, D., "Video Projection Mapping Photogrammetry through Video Tracking," SAE Technical Paper 2013-01-0788, 2013, doi:10.4271/2013-01-0788.
46. Terpstra, T., Voitel, T., and Hashemian, A., "A Survey of Multi- View Photogrammetry Software for Documenting Vehicle Crush," SAE Technical Paper 2016-01-1475, 2016, doi:10.4271/2016-01-1475.
47. Luhmann, T., Stuart, R., Stephen K., and Jan B. *Close-range Photogrammetry and 3D Imaging*. 2nd ed. Walter De Gruyter GmbH, 2014.
48. Jurkofsky, D., "Accuracy of SUAS Photogrammetry for Use in Accident Scene Diagramming," *SAE Int. J. Trans. Safety* 3(2):136–152, 2015, doi:10.4271/2015-01-1426.
49. Carter, N., Hashemian, A., Rose, N., and Neale, W., "Evaluation of the Accuracy of Image Based Scanning as a Basis for Photogrammetric Reconstruction of Physical Evidence," SAE Technical Paper 2016-01-1467, 2016, doi:10.4271/2016-01-1467.
50. Neale, W., Hessel, D., and Terpstra, T., "Photogrammetric Measurement Error Associated with Lens Distortion," SAE Technical Paper 2011-01-0286, 2011, doi:10.4271/2011-01-0286.
51. Wolfgang, H "Correcting lens distortions in digital photographs" http://www.imagemagick.org/Usage/lens/correcting_lens_distortions.pdf.2010.
52. Agisoft PhotoScan (version 1.1.6) http://www.agisoft.com/
53. Wikipedia contributors, "Lens correction model," *Wikipedia, The FreeEncyclopedia*, http://wiki.panotools.org/Lens_correction_model (accessed October 13, 2016).

Contact Information

Toby Terpstra
Kineticorp, LLC
(303) 733-1888
tterpstra@kineticorp.com
www.kineticorp.com

Acknowledgments

The Authors wish to thank:

- Tom Niemann from ePaperPress (PTLens) for his continued support and for providing camera specific lens coefficients for the cameras used in this study.

Definitions/Abbreviations

EXIF - exchangeable image file format

CCD - charged-coupled device

POR - point of rest

LiDAR - a portmanteau of light and radar

RGB - red, green, blue

APPENDIX

APPENDIX A

Figure 20. Photographs used in the study (Kodak Z8612, Olympus C7070 WZ, Samsung ES15)

Figure 21. Uncorrected lens distortion - photogrammetry solutions (Total station data represented by black lines)

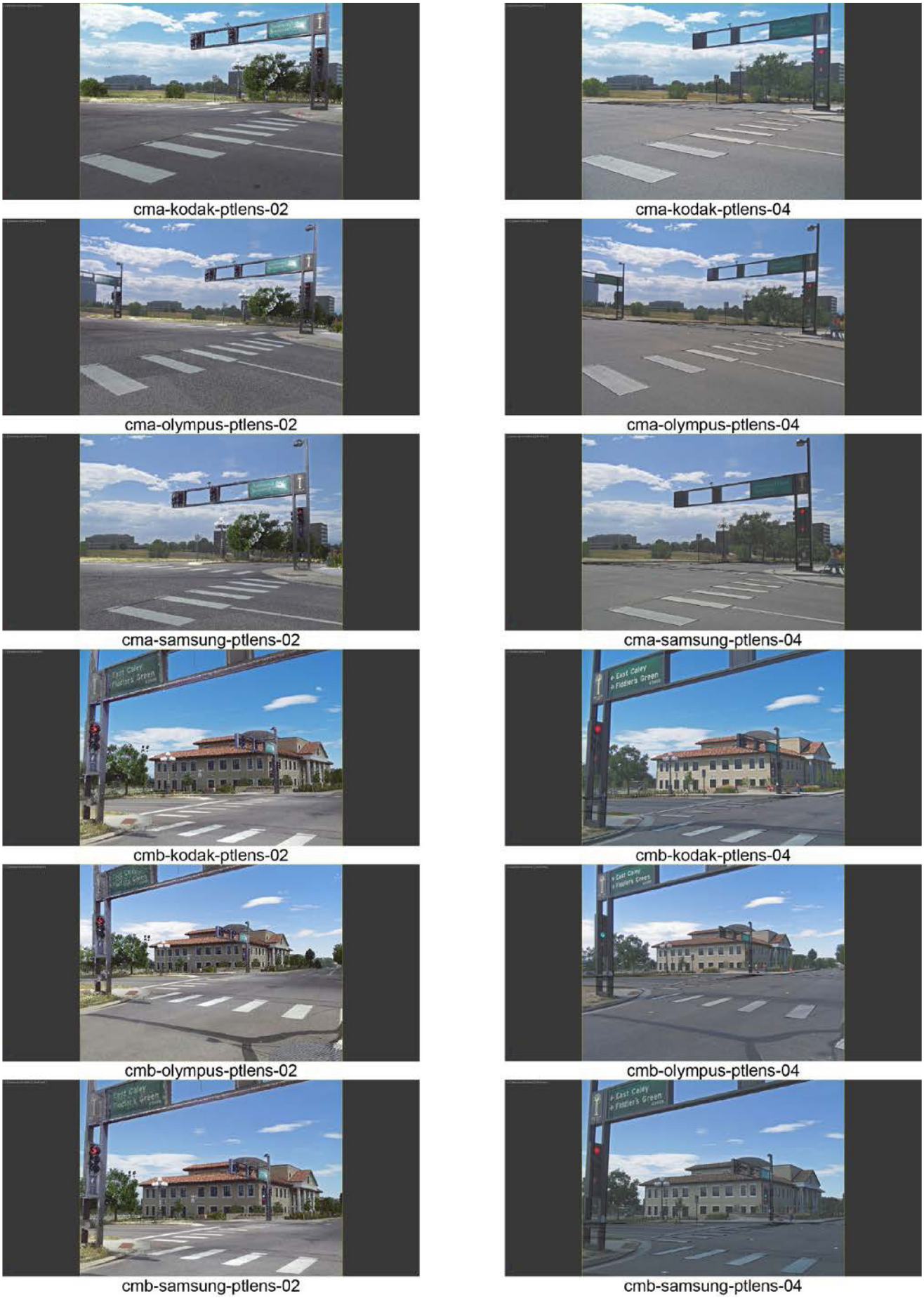

Figure 22. PTLens lens distortion correction - photogrammetry solutions (Point cloud on left, Total station data represented by black lines on right)


cma-kodak-straight-02


cma-kodak-straight-04


cma-olympus-straight-02


cma-olympus-straight-04


cma-samsung-straight-02


cma-samsung-straight-04


cmb-kodak-straight-02


cmb-kodak-straight-04


cmb-olympus-straight-02


cmb-olympus-straight-04


cmb-samsung-straight-02


cmb-samsung-straight-04

Figure 23. Straight-line lens distortion correction - photogrammetry solutions (Point cloud on left, Total station data represented by black lines on right)

Figure 24. Point cloud lens distortion correction - photogrammetry solutions (Point cloud on left, Total station data represented by black lines on right)

APPENDIX B

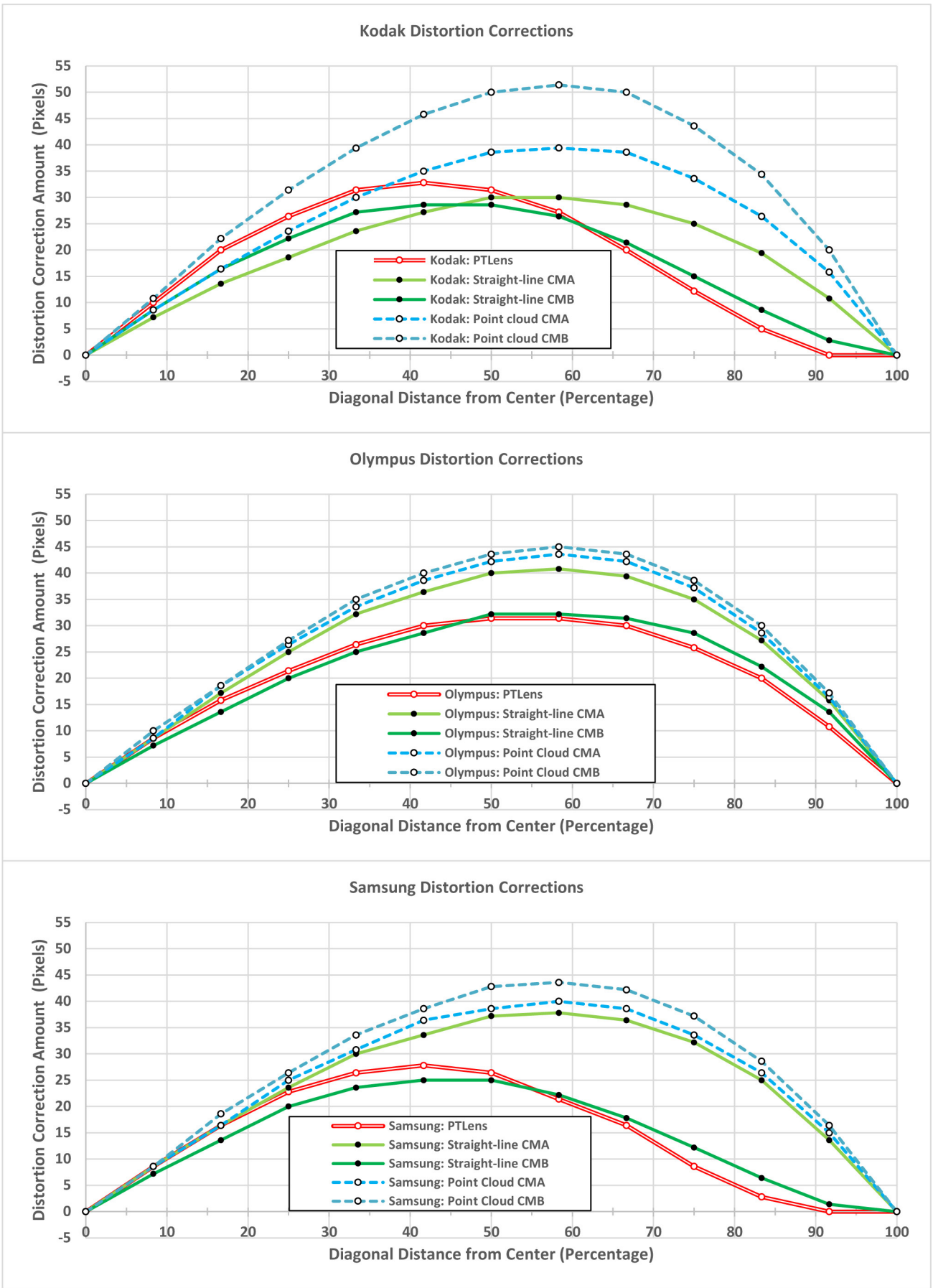

Figure 25. Pixel Movement Comparisons by Camera

Table 8. Pixel Movement Analysis Data: Undistorted Grid Image and PTLens Corrected Grid

Kodak: Undistorted			
	Width	**Height**	**Dist.**
0	0	0	0
1	136	102	170
2	136	102	340
3	136	102	510
4	136	102	680
5	136	102	850
6	136	102	1020
7	136	102	1190
8	136	102	1360
9	136	102	1530
10	136	102	1700
11	136	102	1870
12	136	102	2040
Sum	1632	1224	

Kodak: PTLens				
	Width	**Height**	**Dist.**	**Diff.**
0	0	0	0	0
1	128	96	160	10
2	128	96	320	20
3	131	98	484	26
4	132	99	649	31
5	135	101	817	33
6	137	103	989	31
7	139	105	1163	27
8	142	106	1340	20
9	142	107	1518	12
10	142	106	1695	5
11	140	105	1870	0
12	136	102	2040	0
Sum	1632	1224		216

Olympus: Undistorted			
	Width	**Height**	**Dist.**
0	0	0	0
1	128	96	160
2	128	96	320
3	128	96	480
4	128	96	640
5	128	96	800
6	128	96	960
7	128	96	1120
8	128	96	1280
9	128	96	1440
10	128	96	1600
11	128	96	1760
12	128	96	1920
Sum	1536	1152	

Olympus: PTLens				
	Width	**Height**	**Dist.**	**Diff.**
0	0	0	0	0
1	121	91	151	9
2	122	92	304	16
3	124	92	459	21
4	124	93	614	26
5	125	94	770	30
6	127	95	929	31
7	128	96	1089	31
8	129	97	1250	30
9	131	99	1414	26
10	133	99	1580	20
11	135	102	1749	11
12	137	102	1920	0
Sum	1536	1152		252

Samsung: Undistorted			
	Width	**Height**	**Dist.**
0	0	0	0
1	152	114	190
2	152	114	380
3	152	114	570
4	152	114	760
5	152	114	950
6	152	114	1140
7	152	114	1330
8	152	114	1520
9	152	114	1710
10	152	114	1900
11	152	114	2090
12	152	114	2280
Sum	1824	1368	

Samsung: PTLens				
	Width	**Height**	**Dist.**	**Diff.**
0	0	0	0	0
1	145	109	181	9
2	146	109	364	16
3	147	110	547	23
4	149	112	734	26
5	151	113	922	28
6	153	115	1114	26
7	156	117	1309	21
8	156	117	1504	16
9	158	119	1701	9
10	157	117	1897	3
11	154	116	2090	0
12	152	114	2280	0
Sum	1824	1368		178

Table 9. Pixel Movement Analysis Data: Straight-line Grid

Kodak: Straight-line CMA				
	Width	Height	Dist.	Diff.
0	0	0	0	0
1	130	98	163	7
2	131	98	326	14
3	132	99	491	19
4	132	99	656	24
5	133	100	823	27
6	134	100	990	30
7	136	102	1160	30
8	137	103	1331	29
9	139	104	1505	25
10	140	106	1681	19
11	143	107	1859	11
12	145	108	2040	0
Sum	1632	1224		234

Kodak: Straight-line CMB				
	Width	Height	Dist.	Diff.
0	0	0	0	0
1	129	97	161	9
2	130	97	324	16
3	131	99	488	22
4	132	99	653	27
5	135	101	821	29
6	136	102	991	29
7	138	103	1164	26
8	140	105	1339	21
9	141	106	1515	15
10	141	106	1691	9
11	141	105	1867	3
12	138	104	2040	0
Sum	1632	1224		206

Olympus: Straight-line CMA				
	Width	Height	Dist.	Diff.
0	0	0	0	0
1	121	91	151	9
2	121	91	303	17
3	122	91	455	25
4	122	92	608	32
5	125	93	764	36
6	125	94	920	40
7	127	96	1079	41
8	129	97	1241	39
9	132	98	1405	35
10	134	101	1573	27
11	137	103	1744	16
12	141	105	1920	0
Sum	1536	1152		318

Olympus: Straight-line CMB				
	Width	Height	Dist.	Diff.
0	0	0	0	0
1	122	92	153	7
2	123	92	306	14
3	123	92	460	20
4	124	93	615	25
5	125	94	771	29
6	125	94	928	32
7	128	96	1088	32
8	129	96	1249	31
9	130	98	1411	29
10	133	100	1578	22
11	135	101	1746	14
12	139	104	1920	0
Sum	1536	1152		255

Samsung: Straight-line CMA				
	Width	Height	Dist.	Diff.
0	0	0	0	0
1	145	109	181	9
2	146	109	364	16
3	146	110	546	24
4	147	110	730	30
5	149	112	916	34
6	149	112	1103	37
7	152	113	1292	38
8	153	115	1484	36
9	155	117	1678	32
10	158	118	1875	25
11	161	121	2076	14
12	163	122	2280	0
Sum	1824	1368		294

Samsung: Straight-line CMB				
	Width	Height	Dist.	Diff.
0	0	0	0	0
1	146	110	183	7
2	147	110	366	14
3	147	110	550	20
4	149	112	736	24
5	151	113	925	25
6	152	114	1115	25
7	154	116	1308	22
8	156	116	1502	18
9	156	118	1698	12
10	157	117	1894	6
11	156	117	2089	1
12	153	115	2280	0
Sum	1824	1368		174

Table 10. Pixel Movement Analysis Data: Point Cloud Grid

Kodak: Point cloud CMA				
	Width	**Height**	**Dist.**	**Diff.**
0	0	0	0	0
1	129	97	161	9
2	130	97	324	16
3	130	98	486	24
4	131	98	650	30
5	132	99	815	35
6	133	100	981	39
7	135	102	1151	39
8	137	102	1321	39
9	140	105	1496	34
10	142	106	1674	26
11	144	109	1854	16
12	149	111	2040	0
Sum	1632	1224		306

Kodak: Point cloud CMB				
	Width	**Height**	**Dist.**	**Diff.**
0	0	0	0	0
1	127	96	159	11
2	127	95	318	22
3	129	96	479	31
4	129	98	641	39
5	131	98	804	46
6	133	99	970	50
7	135	101	1139	51
8	137	103	1310	50
9	141	106	1486	44
10	143	108	1666	34
11	148	110	1850	20
12	152	114	2040	0
Sum	1632	1224		399

Olympus: Point Cloud CMA				
	Width	**Height**	**Dist.**	**Diff.**
0	0	0	0	0
1	121	91	151	9
2	120	90	301	19
3	122	91	454	26
4	122	92	606	34
5	124	93	761	39
6	125	94	918	42
7	127	95	1076	44
8	129	97	1238	42
9	132	99	1403	37
10	135	101	1571	29
11	138	103	1744	16
12	141	106	1920	0
Sum	1536	1152		336

Olympus: Point Cloud CMB				
	Width	**Height**	**Dist.**	**Diff.**
0	0	0	0	0
1	120	90	150	10
2	121	91	301	19
3	121	91	453	27
4	122	91	605	35
5	124	93	760	40
6	125	94	916	44
7	127	95	1075	45
8	129	97	1236	44
9	132	99	1401	39
10	135	101	1570	30
11	138	104	1743	17
12	142	106	1920	0
Sum	1536	1152		349

Samsung: Point Cloud CMA				
	Width	**Height**	**Dist.**	**Diff.**
0	0	0	0	0
1	145	109	181	9
2	146	109	364	16
3	145	109	545	25
4	147	111	729	31
5	148	110	914	36
6	150	113	1101	39
7	151	113	1290	40
8	153	115	1481	39
9	156	117	1676	34
10	158	118	1874	26
11	161	121	2075	15
12	164	123	2280	0
Sum	1824	1368		309

Samsung: Point Cloud CMB				
	Width	**Height**	**Dist.**	**Diff.**
0	0	0	0	0
1	145	109	181	9
2	144	108	361	19
3	146	109	544	26
4	146	110	726	34
5	148	111	911	39
6	149	111	1097	43
7	151	114	1286	44
8	153	115	1478	42
9	156	117	1673	37
10	159	119	1871	29
11	162	121	2074	16
12	165	124	2280	0
Sum	1824	1368	14483	337

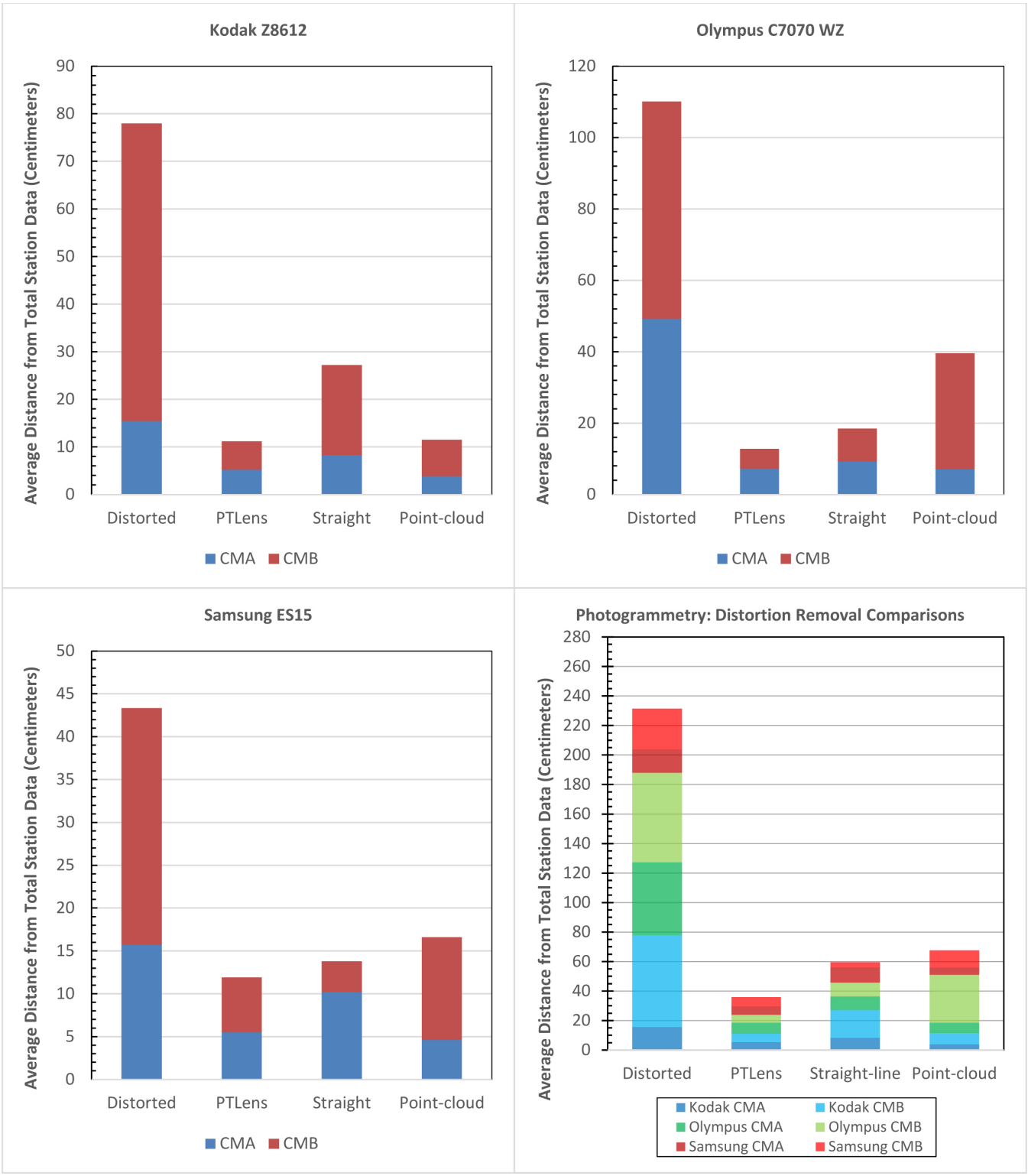

Figure 26. Spray Paint Location Distances from LiDAR Points by Camera and Combined

ISSN 0148-7191

http://papers.sae.org/2017-01-1422